Electronic Supplementary Material (ESI) for Journal of Materials Chemistry A.

Supporting Information

Free-standing Platinum Monolayer as Efficient and Selective Catalyst for Oxygen Reduction Reaction

Arup Mahata,[†] Priyanka Garg,[†] Kuber Singh Rawat,[†] Preeti Bhauriyal,[†] Biswarup Pathak, [†,#,*]

[†]Discipline of Chemistry, School of Basic Sciences and [#]Discipline of Metallurgy Engineering and Materials Science, Indian Institute of Technology (IIT) Indore, Indore, Madhya Pradesh, 453552, India
Email: biswarup@iiti.ac.in

Contents

Table S1: Rate constants values for the elementary reactions

Table S2: Potential dependent activation barriers

Table S3: Reaction free energies of the elementary steps on platene for (a) gas and (b) solvation medium.

Text S1: Computational Details

The first-principles calculations are performed using a projector augmented wave (PAW)[1] method as implemented in the Vienna Ab initio Simulation Package (VASP).[2] The exchange-correlation potential is described by using the generalized gradient approximation of Perdew-Burke-Ernzerhof (GGA-PBE).[3] The PAW method is employed to treat interactions between ion cores and valance electrons.[1] Plane wave with a kinetic energy cut off of 470 eV is used to expand the electronic wave functions. The Monkhorst–Pack generated a set of 45 × 25 × 1 k-points which is used to optimize the unit cell and evaluate the density of states of the Pt-ML. A 3 × 2 × 1 set of k-points has been used in all the calculations where supercell is used. The bulk Pt(111) surface is modeled with a (3 × 3) supercell to minimize the lateral interactions between the repeating images. The metal slab is composed of five atomic layers, where the bottom three layers are fixed and the top two layers are relaxed. A 12 Å of vacuum is used along the z-direction to avoid any periodic interactions. The Brillouin zone is sampled using a 3 × 3 × 1 k-point grid for the surface calculations. All the systems are fully optimized, where the convergence criteria for total energy and forces are set at 10^{-4} eV and <0.02 eV/Å, respectively. Spin-polarized calculations are performed for all the molecular species and oxygen adsorbed intermediates. We have included Grimme's D3-type[4] of semiempirical method to include the dispersion energy corrections for van der Walls interactions. The climbing nudged elastic band (CI-NEB) method[5] is used to locate the transition state. Six intermediate images are used in each CI-NEB pathway. Vibrational frequencies for the initial, transition and final states of the reaction are calculated and the transition states are confirmed by the presence of one imaginary frequency. Zero-point energy (ZPE) is calculated using the following equation:

$$\mathrm{ZPE} = \sum_i 1/2 h\upsilon_i$$

where h is the Planck constant and υ_i is the frequency of the i^{th} vibrational mode. The reaction free energies (ΔG) are calculated using the following equation:

$\Delta G = \Delta E + \Delta ZPE - T\Delta S$

where ΔE, ΔZPE and ΔS are the difference in total energies, zero-point energies and entropy between the product/TS and reactant. The forward (k_i) rate constants for all the elementary steps are calculated using the following equation:

$$k_i = \left(\frac{k_B T}{h}\right)\left(\frac{q_{TS}}{q_R}\right) e^{-\Delta G^{\ddagger}/k_B T}$$

where k_B is the Boltzmann constant, T is the temperature, h is the Plank constant. Here, q_{TS} and q_R are the vibrational partition functions for the transition state and reactant structures, respectively and $\Delta G^{\ddagger}$ is the Gibbs free energy barrier for the initial and final state of the elementary reaction. The finite system (Pt_7 cluster) calculations are carried out using Becke's three-parameter exchange and the Lee−Yang−Parr correlation functional (B3LYP) as implemented in the Gaussian 09 package.[6–9] LANL2DZ basis sets has been used with effective core potentials (ECPs).[10]

References:

(1) Blochl, P. E. Projector augmented-wave method. *Phy. Rev. B* **1994**, *50*, 17953.

(2) (a) Kresse, G.; Hafner, Ab initio molecular dynamics for liquid metals. *J. Phy. Rev. B* **1993**, *47*, 558. (b) Kresse, G.; Hafner, Ab initio molecular-dynamics simulation of the liquid-metal–amorphous-semiconductor transition in germanium. *J. Phy. Rev. B* **1994**, *49*, 14251. (c) Kresse, G.; Joubert, D. From ultrasoft pseudopotentials to the projector augmented-wave method. *Phy. Rev. B* **1999**, *59*, 1758.

(3) Perdew, J. P.; Chevary, J. A.; Vosko, S. H.; Jackson, K. A.; Pederson, M. R.; Singh, D. J.; Fiolhais, C. Atoms, molecules, solids, and surfaces: Applications of the generalized gradient approximation for exchange and correlation. *Phy. Rev. B* **1992**, *46*, 6671.

(4) Grimme, S.; Antony, J.; Ehrlich, S.; Krieg, S. A consistent and accurate ab initio parametrization of density functional dispersion correction (DFT-D) for the 94 elements H-Pu. *J. Chem. Phys.* **2010**, *132*, 154104.

(5) Henkelman, G.; Jonsson, H. Improved tangent estimate in the nudged elastic band method for finding minimum energy paths and saddle points. *J. Chem. Phys.* **2000**, *113*, 9978-9985.

(6) Frisch, M. J.; Trucks, G. W.; Schlegel, H. B.; Scuseria, G. E.; Robb, M. A.; Cheeseman, J. R.; Scalmani, G.; Barone, V.; Mennucci, B.; Petersson, G. A. et al. Gaussian 09, Revision B.01; Gaussian Inc.: Wallingford, CT, 2009.

(7) Becke, A. D. Density-Functional Thermochemistry. III. The Role of Exact Exchange. J. Chem. Phys. 1993, 98, 5648−5652.

(8) Becke, A. D. Density-functional Thermochemistry. IV. A New Dynamical Correlation Functional and Implications for Exact- Exchange Mixing. J. Chem. Phys. 1996, 104, 1040−1046.

(9) Lee, C. T.; Yang, W. T.; Parr, R. G. Development of the Colic- Salvetti Correlation-Energy Formula into a Functional of the Electron Density. Phys. Rev. B: Condens. Matter Mater. Phys. 1988, 37, 785−789.

(10) Hay, P. J.; Wadt, W. R. Ab Initio Effective Core Potentials for Molecular Calculations. Potentials for the Transition Metal Atoms Sc to Hg. J. Chem. Phys. 1985, 82, 270−283.

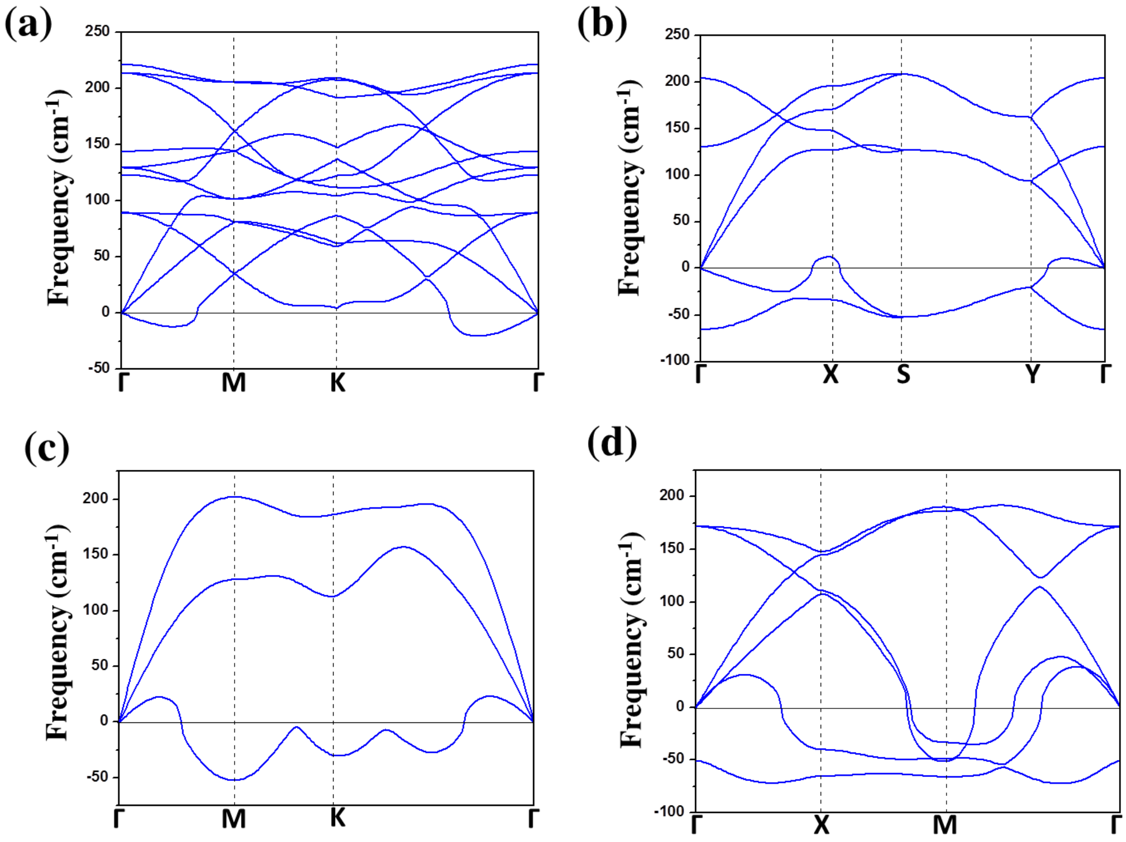

Figure S1: Dispersion of phonon modes for six-coordinated (a) hexagonal buckled, (b) orthorhombic planar, (c) hexagonal planar; and four-coordinated (d) planar.

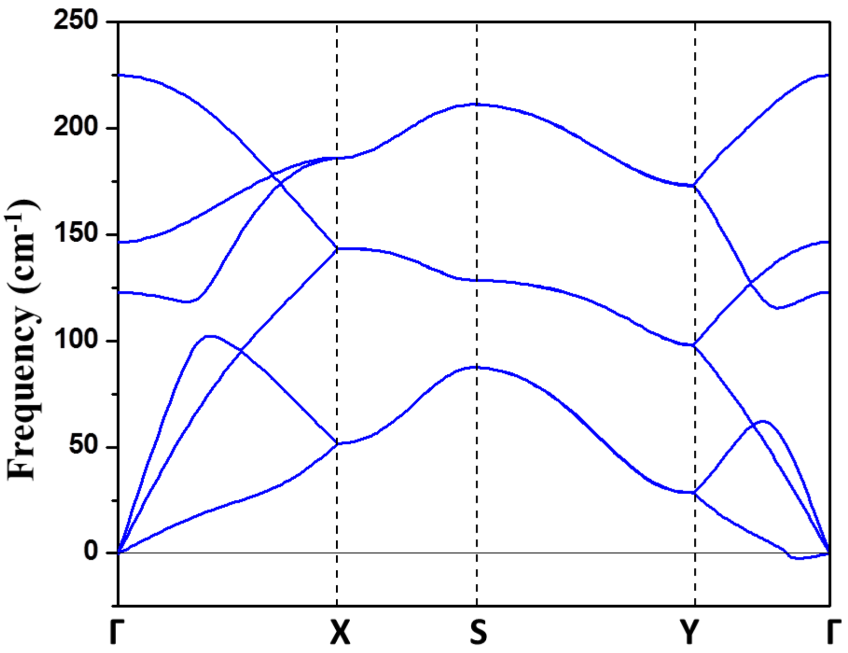

Figure S2: Dispersion of phonon modes of the six-coordinated orthorhombic buckled structure under dielectric effects

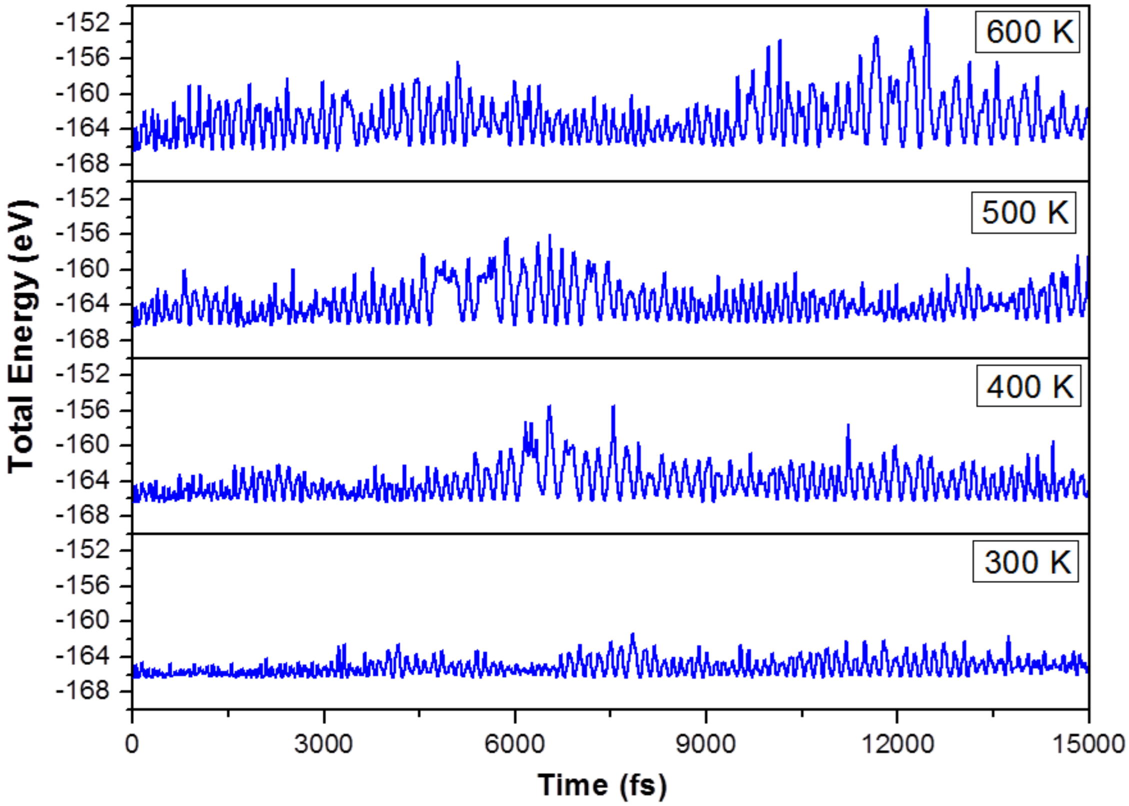

Figure S3: AIMD simulations of platene at different temperatures

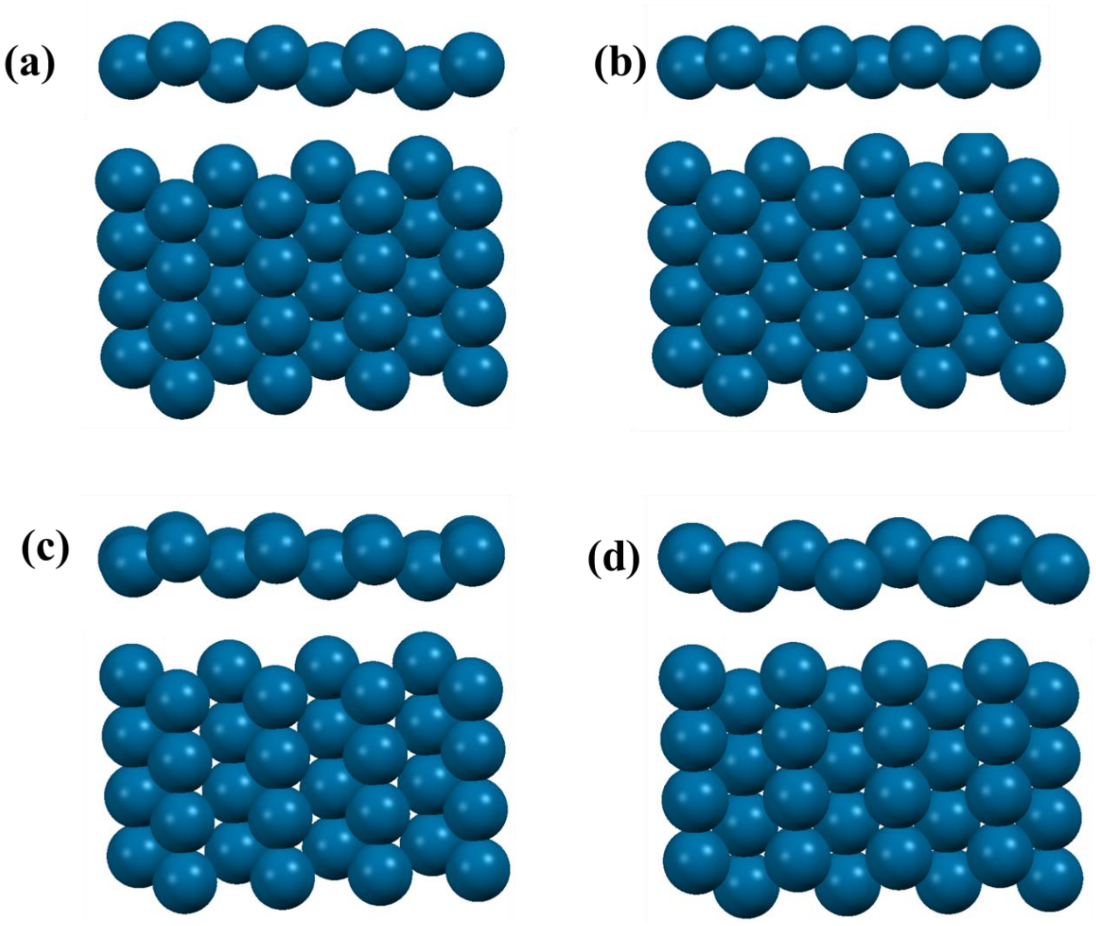

Figure S4: Snapshots of the platene after the end of the simulation at different temperatures: (a) 300, (b) 400, (c) 500 and (d) 600 K.

Text S2: Mechanical properties of platene

For determining the mechanical properties of platene, we have calculated the change of energy in the strain range of -5% to 5% with an increment of 1% by using the standard Voigt notation.[1-2] The elastic strain energy per unit area can be expressed as:[2]

$$\mathrm{U} = 1/2\mathrm{C}_{11}\varepsilon_{\mathrm{xx}}^2 + 1/2\mathrm{C}_{22}\varepsilon_{\mathrm{yy}}^2 + \mathrm{C}_{12}\varepsilon_{\mathrm{xx}}\varepsilon_{\mathrm{yy}} + 2\mathrm{C}_{66}\varepsilon_{\mathrm{xy}}^2 \qquad (1)$$

where C_{11}, C_{22}, C_{12} and C_{66} are the linear elastic constants, whereas $\varepsilon_{\mathrm{xx}}$, $\varepsilon_{\mathrm{yy}}$ and $\varepsilon_{\mathrm{xy}}$are the in-plane stress along the x, y and xy directions, respectively. Elastic constants are second partial derivative of strain energy with respect to strain and can be calculated by polynomial fitting of energy curve in uniaxial and equibiaxial strains.[3] The main criteria for mechanical stability are C11 > C12 and C66 > 0. Our calculated values of C11, C22, C12 and C66 are 164, 120, -30 and 56 GPa.nm, respectively. These are very much comparable with the previously reported values of black phosphorene[4] and borophene[2]. Thus, we can say that platene satisfy all the criteria for mechanical stability. The in-plane Young's modulus (Y) and Poisson's ratio (PR) can be derived from the elastic constants using the following equations[2]

$$E_x = \frac{C_{11}C_{22}-C_{12}C_{21}}{C_{22}}, \ E_y = \frac{C_{11}C_{22}-C_{12}C_{21}}{C_{11}} \qquad (2)$$

$$\upsilon_{xy} = \frac{C_{21}}{C_{22}}, \quad \upsilon_{yx} = \frac{C_{12}}{C_{11}} \qquad (3)$$

Therefore, E_x, E_y and $\upsilon_{xy,}\ \upsilon_{yx}$ are Young's modulus (Y) and Poisson's ratio (PR) in x and y direction, respectively. The calculated values of Y are 164 and 120 GPa.nm, whereas the values of PR are -0.25 and -0.18 in x and y direction, respectively. The calculated values of Y are 164, 120 GPa.nm, whereas the values of PR are -0.25 and -0.18 in x and y direction, respectively. The value of Y is quite lower than the hexagonal graphene (340 GPa.nm)[5] and orthorhombic borophene (398 and 170 GPa.nm)[2]. However, our calculated Y is higher than phosphorene (23 and 92.3 GPa.nm along the armchair and zigzag direction, respectively)[4] and hexagonal stanene monolayer (24 GPa.nm).[6] Moreover, we find that platene possesses negative PR, The negative PR value has been found due to the buckled atomic configuration of platene. The similar kind of observations have been found in the single-layer black phosphorus,[7] borophene[2] and penta-graphene.[1] In fact, Wang et al.[8] also suggested that the negative PR in borophene comes due to the weakening of the interlayer B1–B2 bonding with increasing b-axis strain.

References:

(1) Zhang, S.; Zhou, J.; Wang, Q.; Chen, X.; Kawazoe, Y.; Jena, P. Penta-graphene: A New Carbon Allotrope. *Proc. Natl. Acad. Sci. U. S. A.* **2015**, *112*, 2372−2377.

(2) Mannix, A. J.; Zhou, X.; Kiraly, B.; Wood, J. D.; Alducin, D.; Myers, B. D.; Liu, X.; Fisher, B. L.; Santiago, U.; Guest, J. R.; Yacaman, M. J.; Ponce, A.; Oganov, A. R.; Hersam, M. C.; Guisinger, N. P. Synthesis of Borophenes: Anisotropic, Two-Dimensional Boron Polymorphs, *Science* **2015**, *350*, 1513-1516.

(3) Andrew, R. C.; Mapasha, R. E.; Ukpong, A. M.; Chetty, N. Mechanical Properties of Graphene and Boronitrene. Phys. Rev. B: Condens. Matter Mater. Phys. 2012, 85, 125428.

(4) Wang, L.; Kutana, A.; Zoua, X.; Yakobson, B. I. Electro-mechanical anisotropy of phosphorene, *Nanoscale* **2015**, *7*, 9746-9751.

(5) Lee, C.; Wei, X.; Kysar, J. W.; Hone, J.; Measurement of the elastic properties and intrinsic strength of monolayer graphene. *Science* **2008**, *321*, 385–388.

(6) Tao, L.; Yangy, C.; Wu, L.; Han, L.; Songz, Y.; Wangz, S.; Lu, P.; *Modern Phys. Lett. B*, **2016**, *30*, 1650146

(7) Wei, Q.; Peng, X. Superior Mechanical Flexibility of Phosphorene and Few-Layer Black Phosphorus. *App. Phys. Lett.* **2014**, *104*, 251915.

(8) Wang, H.; Li, Q.; Gao, Y.; Miao, F.; Zhou, X. F.; Wan, X. G. Strain Effects on Borophene: Ideal Strength, Negative Possion's Ratio and Phonon Instability. *New J. Phys.* **2016**, *18*, 073016.

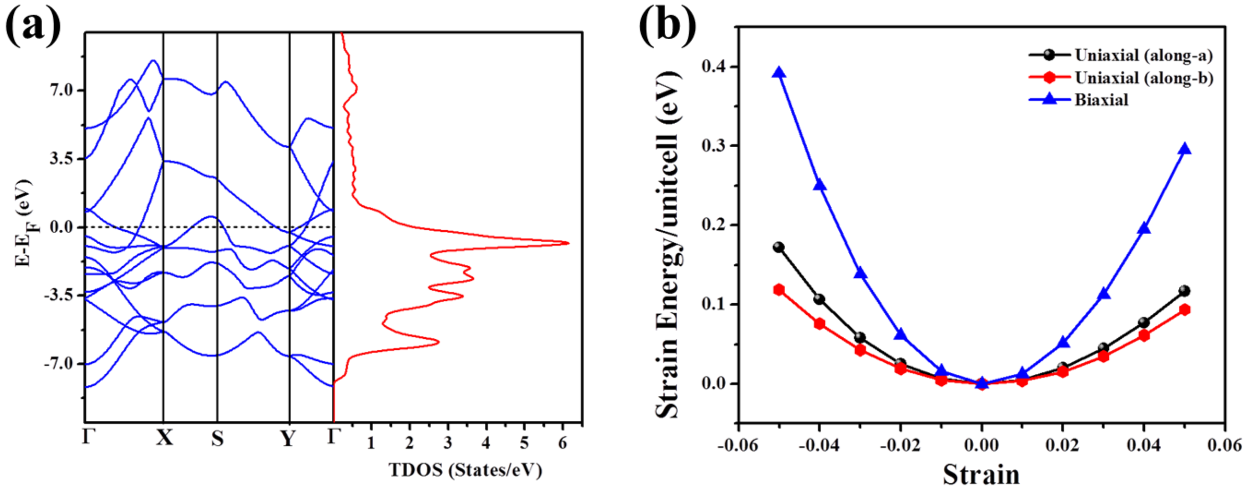

Figure S5: (a) Band structure and total density of states (TDOS) and (b) Strain energy under in-plane uniaxial and biaxial strains of platene.

Text S3: Derivation for the electrode potential shift during Pt dissolution

Dissolution of Pt into the solution proceeds through the following equation.

$Pt \rightarrow Pt^{2+} + 2e^{-}$ (1)

When the dissolution of Pt is referenced to the standard hydrogen electrode (SHE) reaction, the equation (1) can be written as:

$Pt^{n+} + n/2\ H_2 \rightarrow Pt + nH^{+}$ (2).

The Gibbs free energy (ΔG) for this reaction can be written as

$\Delta G = -neU$ (3)

where U is the electrode potential of Pt vs. SHE. Here, n = 2 for the equation (3). Now, considering the platinum in the catalyst and platinum in the solution are in equilibrium, the above equation can be expressed for the monolayer as

$-neU_{Platene} = \mu_{Pt-Platene} + \mu_{nH^{+}} - \mu_{Pt^{n+}} - \mu_{n/2H_2}$ (4)

where $\mu_{Pt-Platene}$, $\mu_{Pt^{n+}}$, $\mu_{nH^{+}}$ and $\mu_{n/2H_2}$ are the chemical potentials of platinum metal, dissolved platinum ions, H^{+} and H_2, respectively.

Similarly, the electrode potential ($U_{Pt(111)}$) of platinum in bulk Pt(111) surface can be related with the chemical potentials using the following equation

$-neU_{Pt(111)} = \mu_{Pt-Pt(111)} + \mu_{nH^{+}} - \mu_{Pt^{n+}} - \mu_{n/2H_2}$ (5)

Therefore, the shift of electrode potential (ΔU) of platinum of NCs with respect to the bulk Pt(111) surface can be written as

$U_{Platene} - U_{Pt(111)} = \Delta U = (\mu_{Pt-Pt(111)} - \mu_{Pt-Platene})/(ne)$ (6)

Now, the chemical potentials of the metal can be defined as

$\mu_{Pt} = \frac{\partial A}{\partial N} \approx \frac{\partial E}{\partial N}$ (7)

where A, E and N are the total free energy, total energy and changes in number of platinum atoms, respectively. The total free energy can be approximated to total energy because the entropic contributions rules out while calculating the chemical potential difference between the metals.

The dissolution of the platinum has been considered by removing one platinum atom from the surface of the catalysts. Hence, the chemical potential of the equation (7) is calculated by considering the defected platene and Pt(111) surface. The chemical potential is obtained by calculating the total energies of the optimized structures (E_{Pt}) and defected structures ($E_{Pt\text{-}def}$).

Therefore, from the equation (7), we can get $\mu_{Pt} = (E_{Pt\text{-}def} - E_{Pt})$

The value of N=1 as only one atom is removed for the calculation.

As the surrounding environment i.e. the presence of O, OH and OOH largely influences the dissolution, the calculation is carried out in the presence of these intermediates.

Therefore, $\mu_{Pt} = (E_{Pt\text{-}def\_O/OH/OOH} - E_{Pt\_O/OH/OOH})$ (8)

We have calculated the chemical potential of platinum for the platene and bulk Pt(111) surface. The atoms, which are removed for the consideration of dissolution behavior at the different sites of the monolayer, have been shown in Figure S6. The value for the bulk Pt(111) surface has been taken from our previous study.[1]

References:

(1) A. Mahata, K. S. Rawat, I. Choudhuri, B. Pathak, *Catal. Sci. Technol.,* 2016, **6**, *7913.*

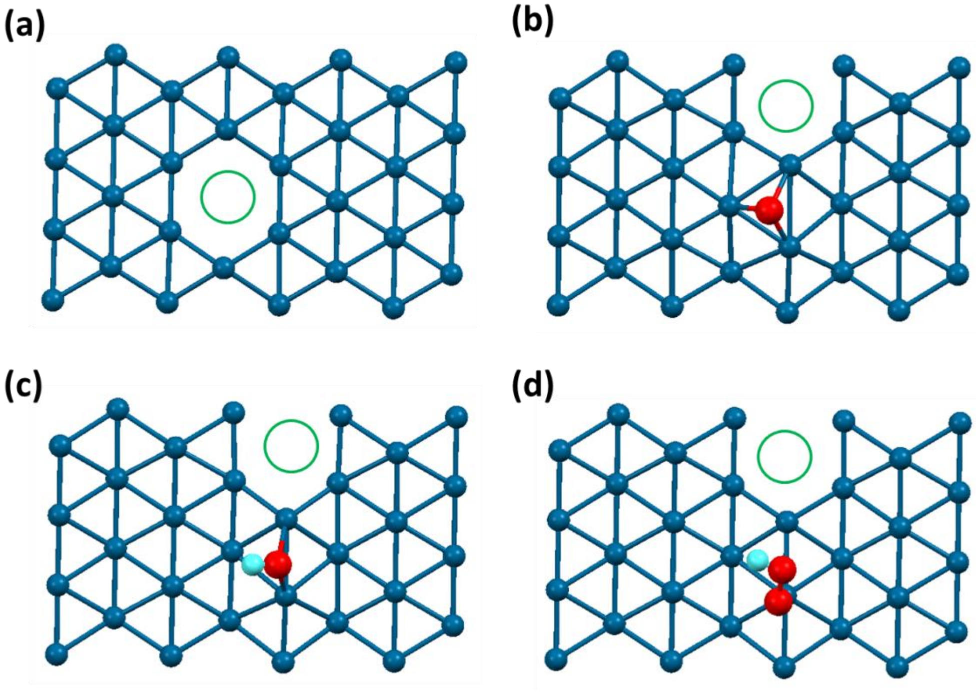

Figure S6: Optimized structures of the defected platene: (a) bare platene, (b) O-adsorbed, (c) OH-adsorbed and (d) OOH adsorbed. The green circle represents the defected site.

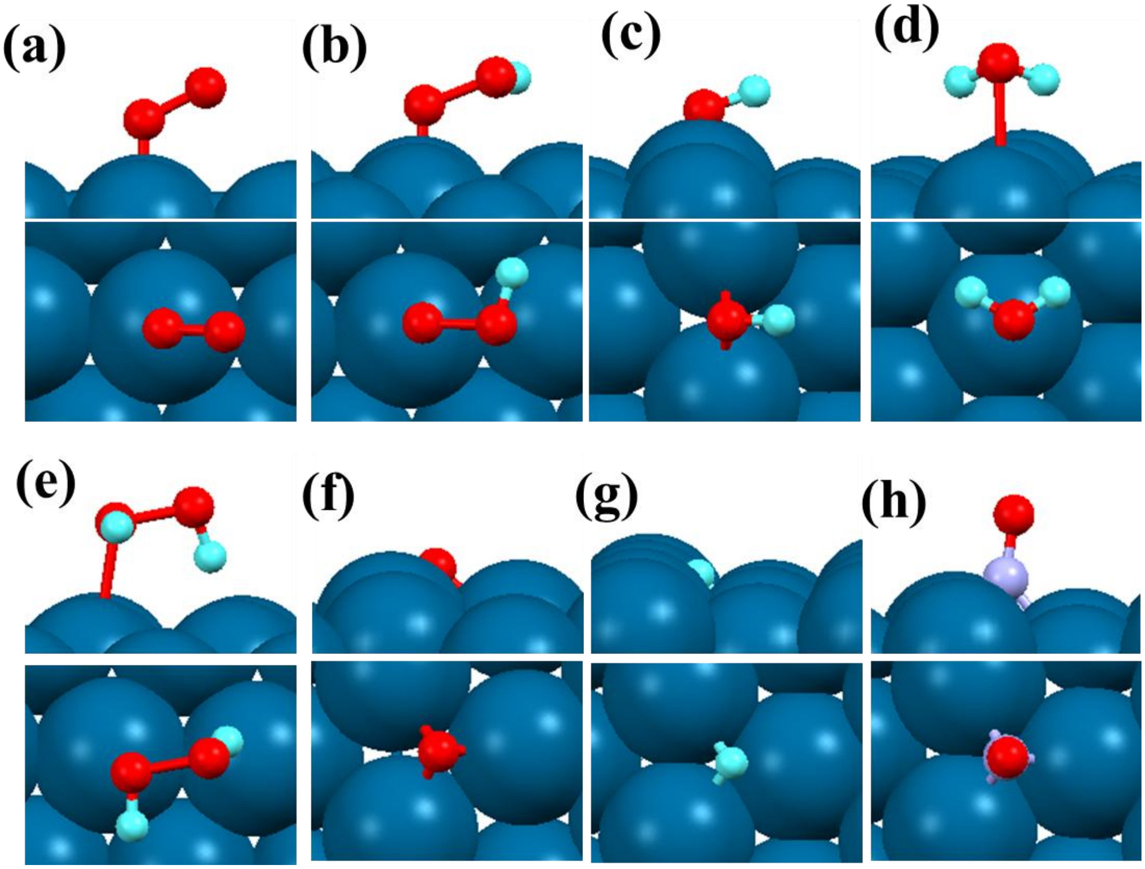

Figure S7: Adsorption behaviours of the intermediates: (a) $*O_2$, (b) *OOH, (c) *OH, (d) $*H_2O$, (e) $*H_2O_2$, (f) *O, (g) *H and (f) *CO.

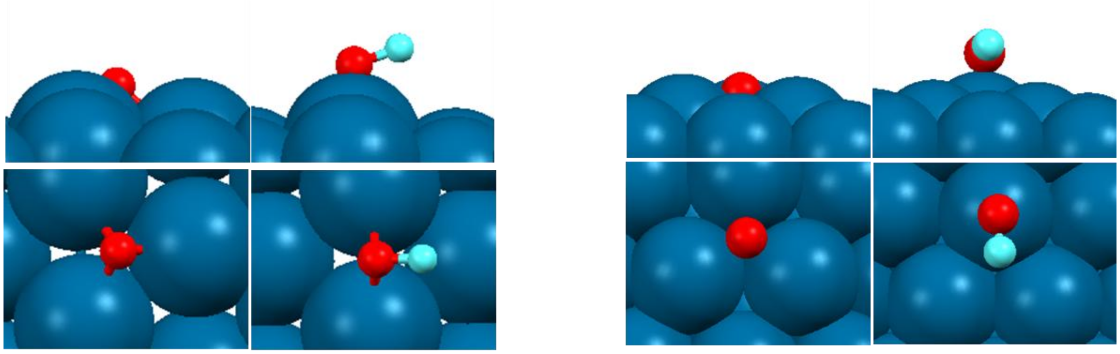

Platene

Bulk Pt(111) surface

Figure S8: Adsorption behaviours of *O and *OH in platene and bulk Pt(111) surface.

Table S1: Rate constants values for the elementary reactions at different temperatures.

Elementary reactions	**300 K**	**400 K**	**500 K**
$*O_2 \rightarrow *O + *O$ (k_1)	1.87×10^{09}	1.94×10^{10}	8.31×10^{10}
$*O_2 + *H \rightarrow *OOH$ (k_2)	2.23×10^{11}	6.98×10^{11}	1.46×10^{12}
$*O + *H \rightarrow *OH$ (k_3)	9.83×10^{10}	3.51×10^{11}	7.93×10^{11}
$*OOH \rightarrow *O + *OH$ (k_4)	3.11×10^{12}	5.30×10^{12}	7.69×10^{12}
$*H + *OOH \rightarrow *H_2O_2$ (k_5)	6.98×10^{11}	1.61×10^{12}	2.80×10^{12}
$*H_2O_2 \rightarrow *OH + *OH$ (k_6)	5.88×10^{12}	8.00×10^{12}	1.01×10^{13}
$*H + *OH \rightarrow *H_2O$ (k_7)	2.42×10^{12}	4.14×10^{12}	6.00×10^{12}

Table S2: Potential dependent activation barriers for *OOH and *OH formation.

Applied Potential (V)	**Activation Barrier (eV)**	
	$*O_2 + H^+ + e \rightarrow *OOH$	**$*O + H^+ + e \rightarrow *OH$**
0.0	-0.07	0.06
0.2	0.17	0.16
0.4	0.27	0.26
0.6	0.37	0.36
0.8	0.47	0.46
1.0	0.57	0.56

Table S3: Reaction free energies of the elementary steps on platene for (a) gas and (b) solvation medium.

Steps	**Elementary Reactions**	**Platene**	
		ΔG(gas phase)	**ΔG(solvation)**
1	$*O_2 \rightarrow *O + *O$ (tilted)	-0.64	-0.67
2	$*O_2 + *H \rightarrow *OOH$	-0.44	-0.67
3	$*O + *H \rightarrow *OH$	-0.42	-0.59
4	$*OOH \rightarrow *O + *OH$	-1.06	-0.96
5	$*OOH + *H \rightarrow *H_2O_2$	-0.61	-0.62
6	$*H_2O_2 \rightarrow *OH + *OH$	-0.72	-0.78
7	$*OH + *H \rightarrow *H_2O$	-1.12	-1.20